

Charge Transfer Effect under Odd-Parity Crystalline Electric Field: Divergence of Magnetic Toroidal Fluctuation in β -YbAlB₄

Shinji Watanabe¹ and Kazumasa Miyake²

¹Department of Basic Sciences, Kyushu Institute of Technology, Kitakyushu, Fukuoka 804-8550, Japan

²Center for Advanced High Magnetic Field Science, Osaka University, Toyonaka, Osaka 560-0043, Japan

A novel property of the quantum critical heavy fermion superconductor β -YbAlB₄ is revealed theoretically. By analyzing the crystalline electronic field (CEF) on the basis of the hybridization picture, odd parity CEF is shown to exist because of sevenfold configuration of B atoms around Yb, which breaks the local inversion symmetry. This allows onsite admixture of 4f and 5d wavefunctions with a pure imaginary coefficient, giving rise to the magnetic toroidal (MT) degree of freedom. By constructing a realistic minimal model for β -YbAlB₄, we show that onsite 4f-5d Coulomb repulsion drives charge transfer between the 4f and 5d states at Yb, which makes the MT fluctuation as well as the electric dipole fluctuation diverge simultaneously with the critical Yb-valence fluctuation at the quantum critical point of the valence transition.

Quantum critical phenomena not following the conventional magnetic criticality¹⁻³⁾ have attracted much attention in condensed-matter physics. The heavy-electron metal β -YbAlB₄ with an intermediate valence of the Yb ion⁴⁾ exhibits a new type of quantum criticality as the magnetic susceptibility $\chi(T) \sim T^{-0.5}$, the specific-heat coefficient $C(T)/T \sim -\log T$, and resistivity $\rho(T) \sim T^{0.5}$ (T for $T \lesssim 1$ K ($T \gtrsim 1$ K)).⁵⁾ Furthermore, the T/B scaling where χ is expressed as a single scaling function of the ratio of the temperature T and magnetic field B over four decades was discovered.⁶⁾ These novel phenomena motivated theoretical studies.⁷⁻¹⁰⁾ The theory of critical Yb-valence fluctuation (CVF) explains not only the quantum criticality in each physical quantity but also the T/B scaling in a unified way.^{8,9)}

Recently, the experimental evidence of the quantum valence criticality has been discovered in α -YbAl_{1-x}Fe_xB₄ ($x = 0.014$).¹¹⁾ The sister compound α -YbAlB₄ shows the Fermi-liquid behavior at low temperatures.⁶⁾ However, by substituting Fe to Al 1.4%, the same unconventional criticality and the T/B scaling as those in β -YbAlB₄ emerges. A remarkable point is that at $x = 0.014$ a sharp Yb-valence crossover occurs that accompanies a sharp change in the volume.¹¹⁾ This provides experimental verification of the theory of the CVF and also valence crossover arising from the quantum critical point (QCP) of the Yb-valence transition.^{8,9)}

The CVF is the charge transfer (CT) fluctuation between the 4f electron at Yb and the conduction electron. In this Letter, we clarify a unique nature of the CT effect under the odd parity crystalline electric field (CEF) arising from local configuration of atoms around Yb in β -YbAlB₄. By constructing the realistic minimal model, we reveal that onsite 4f-5d Coulomb repulsion drives the CT between the 4f and 5d states at Yb, which makes the magnetic toroidal (MT) fluctuation as well as the electric dipole (ED) fluctuation diverge simultaneously with the CVF at the QCP of the valence transition.

Let us start with the CEF in β -YbAlB₄. Since in Yb³⁺ the 4f¹³ configuration is realized and in Yb²⁺ the closed shell appears with the 4f¹⁴ configuration, it is convenient to take the hole picture instead of the electron picture. The ground state of the CEF for the 4f hole state at Yb has been proposed the-

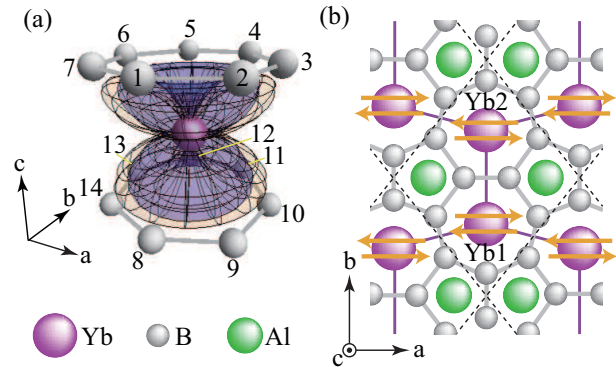


Fig. 1. (color online) (a) Yb surrounded by 7 B rings at upper and lower planes. The squares of absolute values of spherical parts of the 4f ($|J = 7/2, J_z = \pm 5/2\rangle$) wavefunction (orange) and 5d ($|J = 5/2, J_z = \pm 3/2\rangle$) wavefunction (purple) at Yb are also shown. (b) Unit cell is enclosed area by dashed lines. Arrows at Yb represent the MT dipole moments (see text).

oretically to be $|J = 7/2, J_z = \pm 5/2\rangle$,⁷⁾ which accounts for the anisotropy of the magnetic susceptibility. The realization of the $|J = 7/2, J_z = \pm 5/2\rangle$ ground state suggests that the CEF in β -YbAlB₄ is to be understood from the hybridization picture rather than the point-charge model. This view is compatible with the fact that the conical wavefunction of $|J_z = \pm 5/2\rangle$ along the c axis spreads almost toward B rings, which acquires the largest 4f-2p hybridization, as shown in Fig. 1(a).⁷⁾

On the basis of the hybridization picture, let us analyze the CEF at the Yb1 site in the i -th unit cell surrounded by seven B atoms at upper and lower planes in Fig. 1(a) [in the unit cell, there are two equivalent Yb atoms labeled by Yb1 and Yb2, respectively, as shown in Fig. 1(b)]. The point group symmetry at Yb is approximately sevenfold rotation C_7 and hence we take the 2p states at the B site as the basis functions: φ_{p_z} and $\varphi_{p_{\pm}} \equiv (\varphi_{p_x} \pm i\varphi_{p_y})/\sqrt{2}$. The CEF energy of the $|J_z = \pm 5/2\rangle$ state is quantified by the second-order perturbation $\Delta E(\pm 5/2, \pm 5/2) = \langle \pm 5/2 | \frac{H_{ij}^{pf*} H_{ij}^{pf}}{E - H_0} | \pm 5/2 \rangle \equiv \varepsilon_f$ with respect to the 4f-2p

hybridization

$$H_{il}^{pf} = \sum_{\langle i1,j \rangle, m, \sigma, J_z} \left(V_{j m \sigma, i 1 J_z}^{p f} P_{j m \sigma}^\dagger f_{i 1 J_z} + h.c. \right), \quad (1)$$

where $\langle i1, j \rangle$ represents the nearest-neighbor (N.N.) pairs between B sites and the Yb1 site in the i -th unit cell, i.e., $j = 1 \sim 7$ ($8 \sim 14$) for the upper (lower) plane in Fig. 1(a). Here, $m = z, \pm, \sigma = \uparrow, \downarrow$, and $J_z = \pm \frac{5}{2}$.

The microscopic origin of the CVF is considered to be the onsite 4f-5d Coulomb repulsion U_{fd} at Yb. Actually, the first-principles calculation shows that the Yb 5d state contributes to the energy band near the Fermi level E_F .¹² Since the 5d bands are shifted down and forming the wide bandwidth more than 10 eV around E_F ,¹² the high-energy 5d-electron state in an isolate Yb ion within the atomic picture i.e. Hund's rule seems to be relevant to the low-energy state in the hole picture in the crystal. As shown in Fig. 1(a), the 5d wavefunction for $|J = 5/2, J_z = \pm 3/2\rangle$ spreads most closely to the direction to the B rings, which can acquire the largest 5d-2p hybridization among the $J = 5/2$ and $J = 3/2$ manifolds. This is compatible with the hybridization picture mentioned above. Therefore, we proceed our analysis based on the hybridization picture by considering the 4f $|J_z = \pm \frac{5}{2}\rangle$ state and 5d $|J_z = \pm \frac{3}{2}\rangle$ state at Yb site, which will be denoted as $|\pm \frac{5}{2}\rangle_{4f}$ and $|\pm \frac{3}{2}\rangle_{5d}$, respectively, below.

Since the local inversion symmetry at the Yb site is broken owing to the sevenfold configuration of B atoms [see Fig. 1(b)], the odd-parity CEF term can arise. This can be explicitly shown by calculating the off-diagonal term by the second-order perturbation $\Delta E(\pm \frac{3}{2}, \pm \frac{5}{2}) = 5d \langle \pm \frac{3}{2} | \frac{H_{il}^{pd*} H_{il}^{pf}}{E - H_0} | \pm \frac{5}{2} \rangle_{4f}$ with respect to the 5d-2p hybridization

$$H_{il}^{pd} = \sum_{\langle i1,j \rangle, m, \sigma, J_z} \left(V_{j m \sigma, i 1 J_z}^{p d} P_{j m \sigma}^\dagger d_{i 1 J_z} + h.c. \right), \quad (2)$$

for $J_z = \pm \frac{3}{2}$. In the hole picture, by considering the $4f^0$ and an extra 2p hole in vacant states as the intermediate state, $\Delta E(\pm \frac{3}{2}, \pm \frac{5}{2})$ can be calculated as

$$\Delta E(\pm \frac{3}{2}, \pm \frac{5}{2}) = - \sum_{j=1}^{14} \sum_{m \sigma} V_{j m \sigma, i 1 \pm \frac{3}{2}}^{p d*} V_{j m \sigma, i 1 \pm \frac{5}{2}}^{p f} \frac{1 - n_{j m \sigma}^p}{\Delta_0 + \epsilon_{j m \sigma}^p},$$

where $\Delta_0 (> 0)$ is the excitation energy to the $4f^0$ -hole state (i.e., $4f^{14}$ electron state), and $n_{j m \sigma}^p$ and $\epsilon_{j m \sigma}^p$ are the filling and energy of 2p hole, respectively. By inputting the Slater-Koster parameters^{13, 14} to $V_{j m \sigma, i 1 \pm \frac{3}{2}}^{p d*}$ and $V_{j m \sigma, i 1 \pm \frac{5}{2}}^{p f}$ and assuming $n^p = n_{j m \sigma}^p$ and $\epsilon^p = \epsilon_{j m \sigma}^p$ for simplicity, we find that this off-diagonal term is expressed in the form of pure imaginary: $\Delta E(\pm \frac{3}{2}, \pm \frac{5}{2}) = iA$ with A being a real number. We also have

$$\Delta E(\pm \frac{3}{2}, \pm \frac{3}{2}) = 5d \langle \pm \frac{3}{2} | \frac{H_{il}^{pd*} H_{il}^{pd}}{E - H_0} | \pm \frac{3}{2} \rangle_{5d} \equiv \epsilon_d.$$

Then, by diagonalizing the 2×2 matrix $\Delta E_{\pm} = \epsilon_f | \pm \frac{5}{2} \rangle_{4f} \langle \pm \frac{5}{2} | + \epsilon_d | \pm \frac{3}{2} \rangle_{5d} \langle \pm \frac{3}{2} | + iA | \pm \frac{3}{2} \rangle_{5d} \langle \pm \frac{5}{2} | - iA | \pm \frac{5}{2} \rangle_{4f} \langle \pm \frac{3}{2} |$, the CEF ground state is obtained as the Kramers doublet

$$|\Psi_{\pm}\rangle = \left(|u \pm \frac{5}{2}\rangle_{4f} + A |i \pm \frac{3}{2}\rangle_{5d} \right) \frac{1}{\sqrt{u^2 + A^2}}, \quad (3)$$

where u is given by $u = (\epsilon_f - \epsilon_d - \sqrt{(\epsilon_f - \epsilon_d)^2 + 4A^2})/2$.

The admixture of the pure imaginary term in Eq. (3) is also naturally understood from the local geometry around

Yb shown in Fig. 1(b). Since seven B atoms surround each Yb atom symmetrically with respect to the bc plane at which the Yb atom is located, the electric field should work at Yb along the b direction. If we calculate the ED moment $Q_{ilx} \equiv -ex_{i1}$ and $Q_{ily} \equiv -ey_{i1}$, whose operators are given by $Q_{il\zeta} = Q_{il\zeta+} + Q_{il\zeta-}$ for $\zeta = x, y$ with $Q_{ilx+} = -e\frac{5}{7} \sqrt{\frac{3}{10}} d_{i1+\frac{3}{2}}^\dagger f_{i1+\frac{5}{2}} + h.c.$, $Q_{ilx-} = e\frac{5}{7} \sqrt{\frac{3}{10}} d_{i1-\frac{3}{2}}^\dagger f_{i1-\frac{5}{2}} + h.c.$, $Q_{ily+} = -ie\frac{5}{7} \sqrt{\frac{3}{10}} d_{i1+\frac{3}{2}}^\dagger f_{i1+\frac{5}{2}} + h.c.$, and $Q_{ily-} = -ie\frac{5}{7} \sqrt{\frac{3}{10}} d_{i1-\frac{3}{2}}^\dagger f_{i1-\frac{5}{2}} + h.c.$, respectively, by using a general form $|\Psi_{\pm}\rangle = \tilde{u}_{\pm} | \pm \frac{5}{2} \rangle_{4f} + \tilde{v}_{\pm} | \pm \frac{3}{2} \rangle_{5d}$, we obtain $\langle \Psi_{\pm} | Q_{ilx} | \Psi_{\pm} \rangle = e\frac{10}{7} \sqrt{\frac{3}{10}} \text{Re}(\tilde{u}_{\pm}^* \tilde{v}_{\pm})$ and $\langle \Psi_{\pm} | Q_{ily} | \Psi_{\pm} \rangle = -e\frac{10}{7} \sqrt{\frac{3}{10}} \text{Re}(i\tilde{u}_{\pm}^* \tilde{v}_{\pm})$. This implies that when \tilde{u}_{\pm} is a real and \tilde{v}_{\pm} is a pure imaginary, we obtain the symmetrically allowed form as $\langle \Psi_{\pm} | Q_{ilx} | \Psi_{\pm} \rangle = 0$ and $\langle \Psi_{\pm} | Q_{ily} | \Psi_{\pm} \rangle \neq 0$, which is indeed the case of Eq. (3). The ED moment for Eq. (3) is given by $\langle \Psi_{\pm} | Q_{ily} | \Psi_{\pm} \rangle = e\frac{10}{7} \sqrt{\frac{3}{10}} uA / (u^2 + A^2)$.

The result of Eq. (3) indicates that there exists the on-site 4f-5d hybridization, which is usually forbidden in centrosymmetric systems. The odd-parity CEF term is

$$H_{il}^{opCEF} = iA \left(d_{i1+\frac{3}{2}}^\dagger f_{i1+\frac{5}{2}} + d_{i1-\frac{3}{2}}^\dagger f_{i1-\frac{5}{2}} \right) + h.c. \quad (4)$$

Recently, novel multipole degrees of freedom, the MT moment has been defined quantum-mechanically¹⁵⁻¹⁷ as

$$t_l(\mathbf{r}_i) = \frac{\mathbf{r}_i}{l+1} \times \left(\frac{2\mathbf{l}_i}{l+2} + \boldsymbol{\sigma}_i \right) \quad (5)$$

at the site \mathbf{r}_i , where \mathbf{l}_i and $\boldsymbol{\sigma}_i$ are the orbital and spin angular-momentum operators, respectively. In the $| \pm \frac{5}{2} \rangle_{4f} \otimes | \pm \frac{3}{2} \rangle_{5d}$ manifold, the operators of the MT dipole are derived as $T_{il\zeta} = T_{il\zeta+} + T_{il\zeta-}$ for $\zeta = x, y$ with $T_{ilx+} = -i\mu_B \frac{15}{14} \sqrt{\frac{3}{10}} f_{i1+\frac{3}{2}}^\dagger d_{i1+\frac{3}{2}} + h.c.$, $T_{ilx-} = i\mu_B \frac{15}{14} \sqrt{\frac{3}{10}} f_{i1-\frac{3}{2}}^\dagger d_{i1-\frac{3}{2}} + h.c.$, $T_{ily+} = -\mu_B \frac{15}{14} \sqrt{\frac{3}{10}} f_{i1+\frac{3}{2}}^\dagger d_{i1+\frac{3}{2}} + h.c.$, and $T_{ily-} = -\mu_B \frac{15}{14} \sqrt{\frac{3}{10}} f_{i1-\frac{3}{2}}^\dagger d_{i1-\frac{3}{2}} + h.c.$ For the CEF ground state in Eq. (3) we obtain $\langle \Psi_{\pm} | T_{ilx} | \Psi_{\pm} \rangle = \mp \mu_B \frac{15}{7} \sqrt{\frac{3}{10}} uA / (u^2 + A^2)$ and $\langle \Psi_{\pm} | T_{ily} | \Psi_{\pm} \rangle = 0$. The MT moments of the Kramers degenerated states are aligned to the $\pm x$ ($\parallel \pm a$) directions at the Yb1 site as illustrated in Fig. 1(b). Since another Yb atom in the unit cell, Yb2, which has opposite sign of A in Eq. (4), the MT moments are aligned oppositely as shown in Fig. 1(b). At each Yb site, the net MT moment is zero due to the Kramers degeneracy.

On the basis of these analyses, let us construct the Hamiltonian for the periodic crystal of β -YbAlB₄, which consists of the 4f $J_z = \pm 5/2$ and 5d $J_z = \pm 3/2$ states at Yb and $2p_z$ and $2p_{\pm}$ states at B:

$$H = \sum_{i\alpha} \left[H_{i\alpha}^f + H_{i\alpha}^{pf} + H_{i\alpha}^{pd} + H_{i\alpha}^{Ufd} \right] + H^d + H^p, \quad (6)$$

where $\alpha = 1, 2$ specifies the Yb1 and Yb2 sites, respectively. Here, the 4f part is given by $H_{i\alpha}^f = \epsilon_f \sum_{J_z = \pm 5/2} n_{i\alpha J_z}^f + U n_{i\alpha+5/2}^f n_{i\alpha-5/2}^f$, where U is the onsite Coulomb repulsion. The 5d part is given by $H^d = \epsilon_d \sum_i \sum_{\alpha=1,2} \sum_{J_z = \pm 3/2} n_{i\alpha J_z}^d + \sum_{\langle i\alpha, i'\alpha' \rangle} \sum_{J_z, J_z' = \pm 3/2} t_{i\alpha J_z, i'\alpha' J_z'}^{dd} d_{i\alpha J_z}^\dagger d_{i'\alpha' J_z'}$, where $\langle i\alpha, i'\alpha' \rangle$ takes

the N.N. Yb pairs. The 4f-5d Coulomb repulsion at Yb is given by

$$H_{ia}^{U_{fd}} = U_{fd} \sum_{J_z=\pm 5/2} \sum_{J'_z=\pm 3/2} n_{iaJ_z}^f n_{iaJ'_z}^d. \quad (7)$$

The transfer for 2p states is given by $H^P = \sum_{\langle j,j' \rangle \sigma} \sum_{m,m'=\pm} t_{jm,j'm'}^{pp} P_{jm\sigma}^\dagger P_{j'm'\sigma}$, where $\langle j,j' \rangle$ takes the N.N. B pairs in the ab plane and in the c direction [see Fig. 1(a)].

Although H_{ia}^{opCEF} is not included in Eq. (6) explicitly, the effect is expected to inhere via the 2p-4f and 2p-5d hybridizations. To clarify the effect of the CT under the odd-parity CEF, we apply the slave-boson mean-field theory¹⁸⁾ to Eq. (6). To describe the state for $U = \infty$ responsible for heavy electrons, we consider $f_{iaJ_z}^\dagger b_{ia}$ instead of $f_{iaJ_z}^\dagger$ in Eq. (6) by introducing the slave-boson operator b_{ia} to describe the f^0 -hole state and require the constraint $\sum_{ia} \lambda_{ia} (\sum_{J_z=\pm 5/2} n_{iaJ_z}^f + b_{ia}^\dagger b_{ia} - 1)$ with λ_{ia} being the Lagrange multiplier. For $H_{ia}^{U_{fd}}$ in Eq. (6), we employ the mean-field decoupling as $U_{fd} n_{iaJ_z}^f n_{iaJ'_z}^d \approx U_{fd} \bar{n}_\alpha n_{iaJ_z}^f n_{iaJ'_z}^d + R_\alpha n_{iaJ_z}^f - R_\alpha \bar{n}_\alpha$, where $R_\alpha \equiv U_{fd} \bar{n}_\alpha^d$ and $\bar{n}_\alpha \equiv \frac{1}{N} \sum_{iJ_z} \langle n_{iaJ_z}^f \rangle$ ($\eta=f, d$) with N being the number of unit cells. By approximating mean fields as uniform ones, i.e., $\bar{b}_\alpha = \langle b_{ia} \rangle$ and $\bar{\lambda}_\alpha = \lambda_{ia}$, the set of mean-field equations is obtained by $\partial \langle H \rangle / \partial \bar{\lambda}_\alpha = 0$, $\partial \langle H \rangle / \partial \bar{b}_\alpha = 0$, and $\partial \langle H \rangle / \partial R_\alpha = 0$: $\frac{1}{N} \sum_{kJ_z} \langle f_{kaJ_z}^\dagger f_{kaJ_z} \rangle + \bar{b}_\alpha^2 = 1$, $\frac{1}{2N} \sum_k [\sum_{J_z \xi m \sigma} V_{k, \xi m \sigma, \alpha J_z}^{ppf*} \langle f_{kaJ_z}^\dagger P_{k\xi m \sigma} \rangle + h.c.] + \bar{\lambda}_\alpha \bar{b}_\alpha = 0$, and $\bar{n}_\alpha^f = \frac{1}{N} \sum_{kJ_z} \langle f_{kaJ_z}^\dagger f_{kaJ_z} \rangle$. Here, ξ specifies the N.N. B sites for the Yb α site [see Fig. 1(a)]. We solve these equations together with the equation for the filling $\bar{n} \equiv \sum_{\alpha=1,2} (\bar{n}_\alpha^f + \bar{n}_\alpha^d)/4 + \sum_{j=1}^8 \bar{n}_j^p/16$ with $\bar{n}_j^p \equiv \frac{1}{3N} \sum_{km\sigma} \langle P_{kjm\sigma}^\dagger P_{kjm\sigma} \rangle$ self-consistently.

As for the relation among the Slater-Koster parameters, following the argument of the linear combination of atomic orbitals,¹⁹⁾ we set $(pp\pi) = -(pp\sigma)/2$, $(pd\pi) = -(pd\sigma)/\sqrt{3}$, $(pf\pi) = -(pf\sigma)/\sqrt{3}$, $(dd\pi) = -2(dd\sigma)/3$, and $(dd\delta) = (dd\sigma)/6$. In the hole picture, we take the energy unit as $(pp\sigma) = -1.0$ and set $(pd\sigma) = 0.6$, $(pf\sigma) = -0.3$, $(dd\sigma) = 0.4$ as typical values. We found that the calculated band structure for $\varepsilon_d = -1$ and $\varepsilon_f \approx -2.3$ at $\bar{n} = 23/32$ well reproduces the recent photoemission data near E_F ²⁰⁾ and then here we employ these parameters. We performed numerical calculations in the ground state in the $N = 8^3$, 16^3 and 32^3 systems and the results in $N = 32^3$ will be shown below. We confirmed that Eq. (3) with these parameters reproduces the tendency of the anisotropy in the magnetic susceptibility observed in β -YbAlB₄.^{6,21)}

Figure 2(a) shows the ε_f dependence of the 4f-hole number per Yb $\bar{n}^f (= \bar{n}_1^f = \bar{n}_2^f)$. As U_{fd} increases, \bar{n}^f changes steeply as a function of ε_f and for $U_{fd} = 1.40$ the slope $-\partial \bar{n}^f / \partial \varepsilon_f$ diverges at $\varepsilon_f = -2.3001$. Since the valence susceptibility is defined as $\chi_v \equiv -\partial \bar{n}^f / \partial \varepsilon_f$, this result indicates that the CVF diverges $\chi_v = \infty$ at the QCP of the valence transition $(\varepsilon_f^{QCP}, U_{fd}^{QCP}) \approx (-2.3001, 1.40)$. For $U_{fd} > U_{fd}^{QCP}$, a jump in \bar{n}^f appears, indicating the first-order valence transition.

Our realistic minimal model Eq. (6) shows that the QCP with an intermediate valence $\bar{n}^f = 0.71$ as the measurements in β -YbAlB₄⁴⁾ and α -YbAl_{1-x}Fe_xB₄ ($x=0.014$)¹¹⁾ is realized by $U_{fd}^{QCP} = 1.40$. This value is evaluated to be $U_{fd}^{QCP} \approx 6.6$ eV, if we employ the typical value $(pp\sigma) \approx 4.7$ eV estimated from the band-structure calculation in B.²²⁾ Since U_{fd} is the

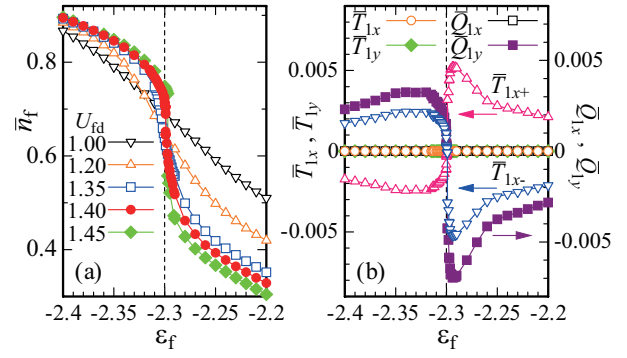


Fig. 2. (color online) (a) The 4f-hole number \bar{n}_f at Yb vs. ε_f for $U_{fd} = 1.00, 1.20, 1.35, 1.40,$ and 1.45 . (b) The ε_f dependences of the MT moment and ED moment at the Yb1 site for $U_{fd} = 1.40$. We set $e = 1$ ($\mu_B = 1$) for the plot of the ED (MT) moment. In (a) and (b), the dashed line indicates $\varepsilon_f = \varepsilon_f^{QCP}$.

onsite interaction, this value seems reasonable. We propose that U_{fd} can be directly examined by recently-developed partial fluorescence yield measurement of the Yb L_3 edge²³⁾ in β -YbAlB₄ and α -YbAl_{1-x}Fe_xB₄ ($x = 0.014$).

Figure 2(b) shows the ε_f dependences of the ED and MT moments at the Yb1 site, which are defined as $\bar{X}_{\alpha\zeta} \equiv \bar{X}_{\alpha\zeta+} + \bar{X}_{\alpha\zeta-}$ with $\bar{X}_{\alpha\zeta\pm} \equiv \frac{1}{N} \sum_i \langle X_{i\alpha\zeta\pm} \rangle$ for $X = Q, T$ and $\zeta = x, y$. The results of $\bar{Q}_{1x} = 0$ and $\bar{Q}_{1y} \neq 0$ indicate that the ED moment along y direction exists. Interestingly, \bar{Q}_{1y} becomes zero in the vicinity of the QCP and changes sign, i.e., $\bar{Q}_{1y} > 0$ ($\bar{Q}_{1y} < 0$) for $\varepsilon_f \lesssim \varepsilon_f^{QCP}$ ($\varepsilon_f \gtrsim \varepsilon_f^{QCP}$), whose absolute value has a maximum at $\varepsilon_f = -2.294 > \varepsilon_f^{QCP}$. The MT moments along x direction for each Kramers state $\bar{T}_{1x\pm}$ also show the sign changes in the vicinity at the QCP, which are also enhanced for $\varepsilon_f > \varepsilon_f^{QCP}$ with opposite signs while $\bar{T}_{1y\pm} = 0$. We note that the relation $|\bar{Q}_{1y}| = \frac{4e}{3\mu_B} |\bar{T}_{1x\pm}|$ holds. Thus the total MT moment is zero $\bar{T}_{1\zeta} = 0$ for $\zeta = x, y$. As for the Yb2 site, we obtained $\bar{Q}_{2x} = 0$, $\bar{Q}_{2y} = -\bar{Q}_{1y}$, $\bar{T}_{2x} = 0$, and $\bar{T}_{2y} = 0$. These results are consistent with the perturbation analysis, which indicates that the odd-parity CEF [see Eq. (4)] is actually generated in Eq. (6).

Although $\bar{T}_\alpha = \mathbf{0}$ is the consequence of the time reversal symmetry of the paramagnetic (PM) state, the MT fluctuation can arise even in the PM state. Then, we calculate the susceptibility of the MT moment

$$\chi_{T_x T_x}(\mathbf{q}, \omega) = \frac{i}{N} \int_0^\infty dt e^{i\omega t} \langle [T_{\mathbf{q}}^x(t), T_{-\mathbf{q}}^x(0)] \rangle \quad (8)$$

with $T_{\mathbf{q}}^x = \sum_i e^{-i\mathbf{q}\cdot\mathbf{r}_i} T_{i1x}$. Figure 3(a) shows the ε_f dependence of $\chi_{MT} \equiv \lim_{\mathbf{q} \rightarrow \mathbf{0}} \chi_{T_x T_x}(\mathbf{q}, 0)$ for $U_{fd} = U_{fd}^{QCP}$. We find that χ_{MT} has a peak at $\varepsilon_f = \varepsilon_f^{QCP}$. This implies that the MT fluctuation is enhanced at the QCP. Since the CVF i.e. CT fluctuation diverges at the QCP, the MT fluctuation is expected to diverge at the QCP if the effect of the CVF is taken into account.

To quantify this beyond the mean-field theory, let us rewrite the MT susceptibility in the form of

$$\chi_{T_x T_x}(\mathbf{q}, \omega) = \frac{9\mu_B^2}{28} \sum_{v=\pm} [\chi_{vv}^{ffdd}(\mathbf{q}, \omega) + \chi_{vv}^{ddff}(\mathbf{q}, \omega)]$$

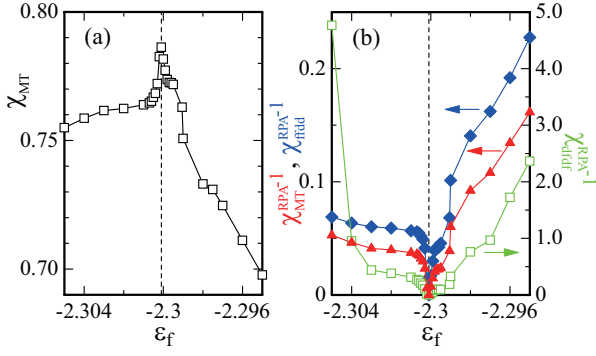


Fig. 3. (color online) (a) χ_{MT} vs. ε_f for $U_{fd} = U_{fd}^{QCP}$. (b) The ε_f dependences of χ_{MT}^{RPA-1} (filled triangle), χ_{fdd}^{RPA-1} (filled diamond), and χ_{dfd}^{RPA-1} (square) for $U_{fd} = U_{fd}^c$ (see text). In (a) and (b), the dashed line indicates $\varepsilon_f = \varepsilon_f^{QCP}$ and we set $\mu_B = 1$.

$$-\chi_{vv}^{dfd}(\mathbf{q}, \omega) - \chi_{vv}^{fdd}(\mathbf{q}, \omega), \quad (9)$$

where $\chi_{vv}^{\beta\gamma\delta\eta}(\mathbf{q}, \omega)$ is defined by $\chi_{vv}^{\beta\gamma\delta\eta}(\mathbf{q}, \omega) \equiv \frac{i}{N} \int_0^\infty dt e^{i\omega t} \langle [\Delta_{qv}^{\beta\delta}(t), \Delta_{qv}^{\gamma\eta}(0)] \rangle$ with $\Delta_{q\pm}^{\beta\delta} = \sum_{\mathbf{k}} \mathbf{k} f_{\mathbf{k}+q1\pm\frac{3}{2}}^\dagger d_{\mathbf{k}1\pm\frac{3}{2}}$ and $\Delta_{q\pm}^{df} = \sum_{\mathbf{k}} d_{\mathbf{k}+q1\pm\frac{3}{2}}^\dagger f_{\mathbf{k}1\pm\frac{3}{2}}$. Since we are currently considering the PM state without applying magnetic field so that $\chi_{++}^{\beta\gamma\delta\eta} = \chi_{--}^{\beta\gamma\delta\eta}$ holds, we omit the index v in the expressions of the susceptibility hereafter. Near the QCP, the CT fluctuation caused by U_{fd} is enhanced,²⁴⁾ which can be calculated by the random phase approximation (RPA) as the corrections for the mean-field state

$$\hat{\chi}(\mathbf{q}, \omega) = \hat{\chi}_0(\mathbf{q}, \omega) \{ \hat{1} - \hat{U} \hat{\chi}_0(\mathbf{q}, \omega) \}^{-1}, \quad (10)$$

where $\hat{\chi}$, $\hat{\chi}_0$, and \hat{U} are given by

$$\hat{\chi}_0(\mathbf{q}, \omega) = \begin{bmatrix} \chi_{(0)}^{fdd}(\mathbf{q}, \omega) & \chi_{(0)}^{fddf}(\mathbf{q}, \omega) \\ \chi_{(0)}^{dfd}(\mathbf{q}, \omega) & \chi_{(0)}^{ddff}(\mathbf{q}, \omega) \end{bmatrix}, \hat{U} = \begin{bmatrix} U_{fd} & 0 \\ 0 & U_{fd} \end{bmatrix},$$

and $\hat{1}$ is the identity matrix. Here, the index 0 specifies the susceptibility calculated for the mean-field state. The critical point within this RPA formalism, defined by the point where $\det\{\hat{1} - \hat{U} \hat{\chi}_0(\mathbf{q}, \omega)\} = 0$ is satisfied, is given by $U_{fd}^c = 1.635$ and $\varepsilon_f = \varepsilon_f^{QCP}$. Then, by substituting $U_{fd} = U_{fd}^c$ and each ε_f in the vicinity of ε_f^{QCP} into Eq. (10) and using the resultant $\chi^{fdd}(\mathbf{q}, \omega) [= \chi^{ddff}(\mathbf{q}, \omega)]$ and $\chi^{dfd}(\mathbf{q}, \omega) [= \chi^{fddf}(\mathbf{q}, \omega)]$, we calculate the ε_f dependence of $\chi_{MT}^{RPA} \equiv \lim_{\mathbf{q} \rightarrow 0} \chi_{TxTx}(\mathbf{q}, 0)$. As shown in Fig. 3(b), the CT fluctuations by $\chi_{fdd}^{RPA} \equiv \lim_{\mathbf{q} \rightarrow 0} \chi^{fdd}(\mathbf{q}, 0)$ and $\chi_{dfd}^{RPA} \equiv \lim_{\mathbf{q} \rightarrow 0} \chi^{dfd}(\mathbf{q}, 0)$ diverge at $\varepsilon_f = \varepsilon_f^{QCP}$, which induce the divergence of the MT fluctuation, i.e., $\chi_{MT}^{RPA} = \infty$.

Since the MT moment is expressed in Eq. (5), it can have a finite matrix element between the 4f and 5d states with the magnetic quantum numbers m and $m \pm 1$, as the ED moment. Hence, the $4f_{\pm\frac{5}{2}}$ and $5d_{\pm\frac{3}{2}}$ states gave the finite values $\bar{T}_{ax\pm}$ and \bar{Q}_{ay} at the locally inversion-symmetry broken Yb site. By the effect of the onsite 4f-5d Coulomb repulsion U_{fd} at Yb, the CT fluctuation is enhanced, which eventually diverges at the valence QCP. This causes the divergences of the MT and ED fluctuations since they consist of the CT fluctuations as Eq. (9), whose operators are expressed as linear combinations of the CT-type operators as $f_{i\alpha\pm\frac{3}{2}}^\dagger d_{i\alpha\pm\frac{3}{2}}$ and its Hermitian con-

jugate. It is also noted that the Yb 5d states, which consist of the spherical harmonics $Y_{2,\pm 2}(\hat{r})$ and/or $Y_{2,\pm 1}(\hat{r})$, can have the finite matrix elements of the MT as well as the ED moment. Hence, the similar effects are expected to appear also for the other 5d states than the $|J = 5/2, J_z = \pm 3/2\rangle$ state.

Since the relation

$$\chi_{Q_y Q_y}(\mathbf{q}, \omega) = \frac{4e^2}{9\mu_B^2} \chi_{TxTx}(\mathbf{q}, \omega) \quad (11)$$

holds where $\chi_{Q_y Q_y}(\mathbf{q}, \omega)$ is defined as $\chi_{Q_y Q_y}(\mathbf{q}, \omega) = \frac{i}{N} \int_0^\infty dt e^{i\omega t} \langle [Q_q^y(t), Q_{-q}^y(0)] \rangle$ with $Q_q^y = \sum_i e^{-iq \cdot r_i} Q_{i1y}$, the ED fluctuation along y is proportional to the MT fluctuation along x . Hence, the ED fluctuation diverges simultaneously with the MT fluctuation at the valence QCP. Although the ED moments at the Yb1 and Yb2 sites [see Fig. 1(b)] are cancelled $Q_{1y} = -Q_{2y}$, their fluctuations exist in the PM state. Equation (11) implies that the measurement of the ED fluctuations by the dielectric constant can detect the MT fluctuation. The detection of the MT as well as ED fluctuation by using various experimental probes such as X-ray diffuse scattering and Mössbauer measurements is an interesting subject in the future.

We also confirmed the tendency that even within the mean field theory, by applying conjugate field to the MT moment $-\sum_{i\alpha} h_\alpha T_{i\alpha x}$ to Eq. (6), $\partial \bar{T}_{\alpha x} / \partial h_\alpha$ diverges at the QCP for a finite h_α . This also supports that the MT fluctuation diverges at the QCP.

In α -YbAl_{1-x}Fe_xB₄, the coincidence of the valence QCP and the magnetic transition seems to occur at $x = 0.014$ as discussed in Ref. 25. This suggests a possibility that the MT order occurs for $x > 0.014$ and the divergence of the uniform MT fluctuation with $\mathbf{q} = \mathbf{0}$ at the QCP affects the MT orders. In β -YbAlB₄, there is also a possibility that the MT order occurs. In that case, it is expected that the MT moment is aligned to $+x$ ($-x$) direction at the Yb1 (Yb2) site, or vice versa, giving the alignment of the staggered MT moments in the ab plane [see Fig. 1(b)].

In summary, by constructing the realistic minimal model for β -YbAlB₄, we have shown that the 4f-5d Coulomb repulsion under the odd parity CEF is the microscopic origin to induce the divergence of the MT fluctuation as well as the ED fluctuation simultaneously with the divergence of the CVF at the QCP of the valence transition. Our study has revealed the underlying mechanism by which novel multipole degrees of freedom can be active as fluctuations, which is a new aspect of the CT effect.

Acknowledgment The authors thank H. Kusunose, S. Hayami, M. Yatsushiro, H. Kobayashi, and C. Bareille for useful discussions. This work was supported by JSPS KAKENHI Grant Numbers JP18K03542, JP18H04326, and JP17K05555.

- 1) T. Moriya, *Spin Fluctuations in Itinerant Electron Magnetism* (Springer-Verlag, Berlin, 1985).
- 2) J. A. Hertz, Phys. Rev. B **14**, 1165 (1976).
- 3) A. J. Millis, Phys. Rev. B **48**, 7183 (1993).
- 4) M. Okawa, M. Matsunami, K. Ishizaka, R. Eguchi, M. Taguchi, A. Chainani, Y. Takata, M. Yabashi, K. Tamasaku, Y. Nishino, T. Ishikawa, K. Kuga, N. Horie, S. Nakatsuji, and S. Shin, Phys. Rev. Lett. **104**, 247201 (2009).
- 5) S. Nakatsuji, K. Kuga, Y. Machida, T. Tayama, T. Sakakibara, Y. Karaki,

- H. Ishimoto, S. Yonezawa, Y. Maeno, E. Pearson, G. G. Lonzarich, L. Balicas, H. Lee, and Z. Fisk, *Nat. Phys.* **4**, 603 (2008).
- 6) Y. Matsumoto, S. Nakatsuji, K. Kuga, Y. Karaki, N. Horie, Y. Shimura, T. Sakakibara, A. H. Nevidomskyy, and P. Coleman, *Science* **331**, 316 (2011).
- 7) A. H. Nevidomskyy and P. Coleman, *Phys. Rev. Lett.* **102**, 077202 (2009).
- 8) S. Watanabe and K. Miyake, *Phys. Rev. Lett.* **105**, 186403 (2010).
- 9) S. Watanabe and K. Miyake, *J. Phys. Soc. Jpn.* **83**, 103708 (2014).
- 10) A. Ramires and P. Coleman, *Phys. Rev. Lett.* **112**, 116405 (2014).
- 11) K. Kuga, Y. Matsumoto, M. Okawa, S. Suzuki, T. Tomita, K. Sone, Y. Shimura, T. Sakakibara, D. Nishio-Hamane, Y. Karaki, Y. Takata, M. Matsunami, R. Eguchi, M. Taguchi, A. Chainani, S. Shin, K. Tamasaku, Y. Nishino, M. Yabashi, T. Ishikawa, and S. Nakatsuji, *Sci. Adv.* **4**, 3547 (2018).
- 12) M. Suzuki and H. Harima, private communications.
- 13) J. C. Slater and G. F. Koster, *Phys. Rev.* **94**, 1498 (1954).
- 14) K. Takegahara, Y. Aoki, and A. Yanase, *J. Phys.: Solid. St. Phys.*, **13**, 583 (1980).
- 15) S. Hayami and H. Kusunose, *J. Phys. Soc. Jpn.* **87**, 033709 (2018).
- 16) S. Hayami, M. Yatsushiro, Y. Yanagi, and H. Kusunose, *Phys. Rev. B* **98**, 165110 (2018).
- 17) H. Watanabe and Y. Yanase, *Phys. Rev. B* **96**, 064432 (2017).
- 18) Y. Onishi and K. Miyake, *J. Phys. Soc. Jpn.* **69**, 3955 (2000).
- 19) O. K. Andersen and O. Jepsen, *Physica B* **91**, 317 (1977).
- 20) C. Bareille, S. Suzuki, M. Nakayama, K. Kuroda, A. H. Nevidomskyy, Y. Matsumoto, S. Nakatsuji, T. Kondo, and S. Shin, *Phys. Rev. B* **97**, 045112 (2018).
- 21) Y. Matsumoto, K. Kuga, T. Tomita, Y. Karaki, and S. Nakatsuji, *Phys. Rev. B* **84**, 125126 (2011).
- 22) D. A. Papaconstantopoulos, *Handbook of the Band Structure of Elemental Solids* (Springer US, 2015).
- 23) H. Tonai, N. Sasabe, T. Uozumi, N. Kawamura, and M. Mizumaki, *J. Phys. Soc. Jpn.* **86**, 093704 (2017).
- 24) K. Miyake, *J. Phys.: Condens. Matter* **19**, 125201 (2007).
- 25) S. Watanabe and K. Miyake, *J. Phys.: Condens. Matter* **23**, 094217 (2011).